Energy-balancing dual-port grid-forming control for VSC-HVDC systems

Conference Paper

Author(s):
Subotic, Irina ; Gross, Dominic

Energy-balancing dual-port grid-forming control for VSC-HVDC systems

Irina Subotić * **Dominic Groß** **

* *Automatic Control Laboratory, ETH Zürich, Switzerland*
(e-mail:subotici@ethz.ch).
** *Department of Electrical and Computer Engineering, University of*
Wisconsin-Madison, USA; e-mail (e-mail: dominic.gross@wisc.edu)

Abstract: This work examines energy-balancing dual port grid-forming (GFM) control for high-voltage direct current (HVDC) transmission. In contrast to the state-of-the-art, HVDC converters controlled in this way do not require assigning GFM and grid-following roles to different converters. Moreover, this control enables primary frequency control and inertia support through HVDC links. A detailed stability and steady-state analysis results in conditions on the control gains such that i) the overall hybrid dc/ac system is stable, ii) asynchronous ac areas are quasi-synchronous, and iii) circulating power in cyclic topologies is avoided. Finally, a high-fidelity case study is used to illustrate and verify the analytical results.

Keywords: Power systems, Power systems stability, Grid-forming control, HVDC transmission

1. INTRODUCTION

Due to their ability to transfer power across long distances and underwater, the use of high voltage direct current (HVDC) transmission is increasing worldwide and significantly impacts the operation and dynamics of power systems. In particular, the use of voltage source converters (VSCs) in HVDC transmission systems has resulted in power systems containing multiple high voltage alternating current (HVAC) systems interconnected by point-to-point VSC-HVDC links. For example, the European power grid consists of five main synchronous areas/regions operating with a nominal frequency of 50 Hz with asynchronous interconnections through point-to-point HVDC links (Hertem et al., 2016). The fast and flexible response of power converters also allows for segmenting such power systems into several ac systems and control the power flow between individual synchronous areas to reduce the risk of cascading outages and blackouts (Mousavi et al., 2013).

State-of-the-art dc/ac power converter controls can be broadly categorized into grid following (GFL) and grid forming (GFM) control for the converter ac and dc terminals (Gomis-Bellmunt et al., 2021). Specifically, ac-GFL/dc-GFM control stabilizes the dc terminal voltage but crucially requires a stable ac terminal voltage (i.e., frequency and magnitude) and can destabilize the system if the ac grid voltage is not tightly controlled by another unit. In contrast, ac-GFM/dc-GFL control imposes a well-defined and stable ac voltage waveform on the grid and provides primary frequency control (Chandorkar et al., 1993; D'Arco et al., 2015) but can destabilize the system if the dc voltage is not tightly controlled by a dc source or other converter (Tayyebi et al., 2020). In contrast, the so-called dual-port GFM control is ac-GFM/dc-GFM, i.e., it simultaneously imposes a well-defined ac voltage and stabilizes the dc terminal voltage while ensuring power balancing between the ac and dc terminals. A key feature of this control is that it subsumes standard functions of well-known ac-GFM/dc-GFL and ac-GFL/dc-GFM controls for renewable generation (Lyu et al., 2022) and enables

bidirectional grid support through HVDC systems (Groß et al., 2022). In particular, stabilizing the dc voltage implies stabilizing the ac frequency and vice-versa.

Using standard controls for VSC-HVDC, a mix of ac-GFL/dc-GFM and ac-GFM/dc-GFL controls is needed to operate a mix of HVAC and HVDC transmission (Gomis-Bellmunt et al., 2021). For example, for a point-to-point HVDC link at least one ac-GFL/dc-GFM VSC is needed to stabilize the dc grid and an ac-GFM/dc-GFL VSC may be needed to stabilize the ac grid (e.g., an offshore windfarm). Assigning control roles to HVDC-VSCs is not a trivial task and results in significant system complexity. Moreover, both ac-GFL and dc-GFL controls are vulnerable to changes in the subsystem topologies (loss of a line and/or generator) or primary control reserves (e.g., due to contingencies). To address these challenges, dual-port GFM control can be applied to VSC-HVDC systems (Groß et al., 2022). In this case, i) no assignment of control roles is required, ii) the system complexity is reduced, iii) the system is more resilient, and iv) primary frequency control and inertia support through HVDC systems are enabled. However, stability conditions and rigorous steady-state analysis for VSC-HVDC systems using dual-port GFM control are not available in the literature.

The main contribution of this work is detailed stability and steady-state analysis. In particular, we provide conditions on the control gains of dual-port GFM controlled HVDC converters that ensure frequency and dc voltage stability. Additionally, we provide conditions on the control gains such that i) ac areas connected through HVDC links are quasi-synchronous, and ii) circulating power flows are eliminated in steady state. Finally, the analytical results are illustrated using a high-fidelity case study.

Notation

The set of real and natural numbers is denoted with $\mathbb{R}$ and $\mathbb{N}$ and we define $\mathbb{R}_{\geq a} := \{x \in \mathbb{R} | x \geq a\}$. For column vectors $x \in \mathbb{R}^n$ and $y \in \mathbb{R}^m$ we use $(x, y) = [x^\mathsf{T}, y^\mathsf{T}]^\mathsf{T} \in \mathbb{R}^{n+m}$ to

denote a stacked vector. Zero matrices of dimension $n \times m$ are denoted by $\mathbb{0}_{n \times m}$, I_n denotes the identity matrix of dimension n, $\mathbb{0}_n$ and $\mathbb{1}_n$ denote column vectors of zeros and ones of length n, and $\otimes$ denotes the Kronecker product.

2. POWER SYSTEM MODEL

In this section, we introduce a reduced-order model of the power system shown in Fig. 1 that consists of i) power transmission, ii) power conversion, and iii) power generation. The aggregate frequency dynamics of each ac area are represented by a single aggregate synchronous generator. This model is justified for today's legacy systems that largely depend on conventional synchronous generators.

2.1 Power transmission

To each ac bus we assign a voltage phase angle $\theta_l \in \mathbb{R}$, a frequency $\omega_l \in \mathbb{R}$, and an ac voltage magnitude $V_l \in \mathbb{R}_{>0}$. To each dc bus we assign a dc voltage $v_l \in \mathbb{R}_{>0}$. We consider quasi-steady-state power flow models linearized around $V_l^\star = V_k^\star = V^\star$ and $v_l^\star = v_k^\star = v_{lk}^\star$ (cf. (Sauer and Pai, 1998)). Thus, all variables denoted by $(\cdot)_\delta$ represent deviations from the nominal operating points denoted by $(\cdot)^\star$, e.g., $\theta_{\delta,l} := \theta_l - \theta_l^\star$. This results in the active ac and dc power flows

$$P_{ac,\delta,l} = \tilde{b}_{lk}^{ac}(\theta_{\delta,l} - \theta_{\delta,k}), \quad P_{dc,\delta,l} = \tilde{g}_{lk}^{dc}(v_{\delta,l} - v_{\delta,k}), \quad (1)$$

where $\tilde{b}_{lk}^{ac} := V^\star V^\star b_{lk}^{ac}$ and $\tilde{g}_{lk}^{dc} := v_{lk}^\star g_{lk}^{dc}$, and $b_{lk}^{ac} \in \mathbb{R}_{>0}$ and $g_{lk}^{dc} \in \mathbb{R}_{>0}$ are the ac succeptance, and dc conductance.

2.2 Power conversion

We consider two power conversion devices: i) synchronous machines (SM) that transform mechanical to electrical power, and ii) two-level dc/ac voltage source converters (2L-VSC) that transform dc to ac power. Using $J_l \in \mathbb{R}_{>0}$, $\omega_l^\star \in \mathbb{R}_{>0}$, and $P_{g,\delta,l} \in \mathbb{R}$, to denote the inertia constant, nominal machine frequency, and mechanical power applied to the machine, results in the synchronous machine model

$$\frac{d}{dt}\theta_{g,\delta,l} = \omega_{\delta,l}, \quad (2a)$$

$$J_l \omega_l^\star \frac{d}{dt}\omega_{\delta,l} = P_{g,\delta,l} - P_{\Sigma,\delta,l}, \quad (2b)$$

where $P_{\Sigma,\delta,1} = -P_{ac,\delta,1} - P_{ac,\delta,3} + P_{ac,\delta,5} - P_{ac,\delta1} + P_{d,1}$ and $P_{\Sigma,\delta,2} = -P_{ac,\delta,2} - P_{ac,\delta,4} - P_{ac,\delta,5} + P_{d,2}$ denote the power injection of the SMs, and, for $l \in \{1,2\}$, $P_{d,l}$ models load variations in the ac areas.

While our results also apply to more complex converter topologies (cf. (Groß et al., 2022)), for the brevity of the presentation, we consider a lossless averaged 2L-VSC model with dc-link charge dynamics (cf. (Groß et al., 2022; Subotić and Groß, 2022))

$$c_l v_{lk}^\star \frac{d}{dt}v_{\delta,l} = -P_{ac,\delta,l} - P_{dc,\delta,l}, \quad (3)$$

where $c_l \in \mathbb{R}_{>0}$ is the dc-link capacitance. The 2L-VSC typically tracks references for $V_{\delta,l} \in \mathbb{R}_{>0}$ and $\theta_{\delta,l} \in \mathbb{R}$. In this study we assume that $V_{\delta,l}$ is given by standard $Q - V$ droop control (D'Arco et al., 2015) and $\theta_{\delta,l} \in \mathbb{R}$ remains as a control input for dual-port GFM control (see Sec. 3).

2.3 Power generation

The conventional turbine-governor system of, e.g., a steam turbine, is modeled by the first-order model (cf. (Sauer and Pai, 1998))

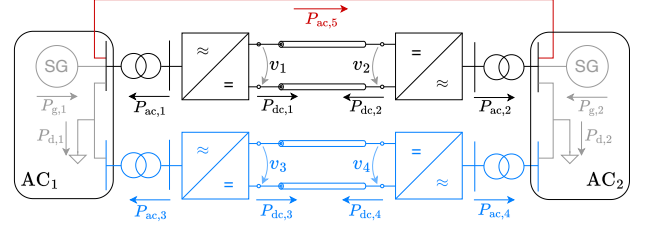$$T_{g,l}\frac{d}{dt}P_{g,\delta,l} = -P_{g,\delta,l} - k_{g,l}\omega_{\delta,l} \quad (4)$$

Fig. 1. Two ac areas (gray) connected through: i) HVDC link (black), ii) second HVDC link (blue), and iii) HVAC transmission line (red).

with turbine time constant $T_{g,i} \in \mathbb{R}_{>0}$ and governor gain $k_{g,l} \in \mathbb{R}_{\geq 0}$. Notably, if $k_{g,l} = 0$, the turbine does not contribute to primary frequency control.

3. ENERGY BALANCING DP-GFM CONTROL

In contrast to standard HVDC converter control (i.e., ac-GFM/dc-GFL and ac-GFL/dc-GFM), we investigate an energy balancing DP-GFM control, that simultaneously imposes stable ac voltage (i.e., frequency and magnitude) and stabilizes its dc terminal voltage. The controller computes the ac voltage phase angle $\theta_{\delta,l}$ as the integral of

$$\omega_{\delta,l} = k_{p,l}\frac{d}{dt}v_{\delta,l} + k_{\omega,l}v_{\delta,l}. \quad (5)$$

The derivative and proportional feedback gains from the dc voltage to the ac frequency are denoted with $k_{p,l} \in \mathbb{R}_{>0}$ and $k_{\omega,l} \in \mathbb{R}_{>0}$. The proportional gain $k_{\omega,l}$ is typically tuned to shape the steady-state response while the derivative gain $k_{p,l}$ shapes the transient response (see Sec. 5).

The key feature of the proposed controller is that it maps the signals indicating power imbalance on the dc terminal (i.e., dc voltage) to the ac terminal (i.e., ac frequency) and vice-versa. Thus, using (5) control for HVDC-VSCs: i) a frequency deviation in an ac area induces a frequency deviation in an ac area connected through the HVDC link, allowing both areas to provide a primary frequency control and inertia response and ii) stability can be guaranteed if, at any time, one of the ac areas has sufficient primary control reserves.

3.1 Overall linearized model

To obtain the overall system model, we combine the reduced-order device models (Sec. 2) and change coordinates from bus voltage angles to angle differences across HVAC lines (Monshizadeh et al., 2017, cf. Sec. III). After the change of coordinates, identical bus angles (i.e., $\theta_{g,\delta,1} = \theta_{\delta,1}$) correspond to zero angle differences (i.e., $\eta_{\delta,1} = \theta_{g,\delta,1} - \theta_{\delta,1} = 0$). Next, let $x_\delta := (\eta_\delta, \omega_\delta, v_\delta, P_{g,\delta}) \in \mathbb{R}^{13}$ with $\eta_\delta := (\theta_{g,\delta,1} - \theta_{g,\delta,2}, \theta_{g,\delta,1} - \theta_{\delta,1}, \theta_{g,\delta,1} - \theta_{\delta,3}, \theta_{g,\delta,2} - \theta_{\delta,2}, \theta_{g,\delta,2} - \theta_{\delta,4}) \in \mathbb{R}^5$, $\omega_\delta := (\omega_{\delta,1}, \omega_{\delta,2}) \in \mathbb{R}^2$, $v_\delta := (v_{\delta,1}, v_{\delta,3}, v_{\delta,2}, v_{\delta,4}) \in \mathbb{R}^4$, $P_{g,\delta} := (P_{g,\delta,1}, P_{g,\delta,2}) \in \mathbb{R}^2$, and $P_{d,\delta} := (\mathbb{0}_5, P_{d,\delta,1}, P_{d,\delta,2}, \mathbb{0}_6) \in \mathbb{R}^{13}$. Then, the overall power system model is given by

$$T \frac{d}{dt}x_\delta = Ax_\delta - P_{d,\delta} \quad (6)$$

and $T := \text{blkdiag}\{I_5, M, C, T_g\}$. Moreover, we define $T_g := \{T_{g,l}\}_{l=1}^2$, $M := \text{diag}\{\omega_l^\star J_l\}_{l=1}^2$, $K_g := \{k_{g,l}\}_{l=1}^2$, $C := \text{diag}\{v_{12}^\star c_1, v_{34}^\star c_3, v_{12}^\star c_2, v_{34}^\star c_4\}$, $K_\omega := \{k_{\omega,1}, k_{\omega,3}, k_{\omega,2}, k_{\omega,4}\}$, $\mathcal{W}_{ac} := \text{diag}\{\tilde{b}_{12}^{ac}, \tilde{b}_{11}^{ac}, \tilde{b}_{13}^{ac}, \tilde{b}_{22}^{ac}, \tilde{b}_{24}^{ac}\}$, $\tilde{K} := \text{diag}\{0, K_p C^{-1}\}$ with $K_p := \text{diag}\{k_{p,1}, k_{p,3}, k_{p,2}, k_{p,4}\}$, the dc Laplacian $L_{dc} = B_{dc}\text{diag}\{\tilde{g}_{12}^{dc}, \tilde{g}_{34}^{dc}\}B_{dc}^\mathsf{T}$, and

$$B_{\mathrm{dc}} := \begin{bmatrix} 1 & 0 & -1 & 0 \\ 0 & 1 & 0 & -1 \end{bmatrix}^{\mathsf{T}}, \ \mathcal{I}_1^{\mathsf{T}} := \begin{bmatrix} 1 & 1 & 1 & 0 & 0 \\ -1 & 0 & 0 & 1 & 1 \end{bmatrix}, \ \mathcal{I}_2^{\mathsf{T}} := [\mathbb{0}_4 \ I_4].$$

Then, $A \in \mathbb{R}^{13 \times 13}$ is given by

$$A := \begin{bmatrix} -\tilde{K}\mathcal{W}_{\mathrm{ac}} & \mathcal{I}_1 & \mathcal{I}_2(K_p C^{-1} L_{\mathrm{dc}} - K_\omega) & \mathbb{0}_{5 \times 2} \\ -\mathcal{I}_1^{\mathsf{T}}\mathcal{W}_{\mathrm{ac}} & \mathbb{0}_{2 \times 2} & \mathbb{0}_{2 \times 4} & I_2 \\ \mathcal{I}_2^{\mathsf{T}}\mathcal{W}_{\mathrm{ac}} & \mathbb{0}_{4 \times 2} & -L_{\mathrm{dc}} & \mathbb{0}_{4 \times 2} \\ \mathbb{0}_{2 \times 4} & -K_{\mathrm{g}} & \mathbb{0}_{2 \times 4} & -I_2 \end{bmatrix}.$$

4. STEADY-STATE FREQUENCY MAPPING

In this section, we analyze the steady-state of the system shown in Fig. 1 with a focus on circulating power flows.

4.1 Steady-states

Setting $\frac{\mathrm{d}}{\mathrm{d}t} x_\delta = 0$ in (6) we obtain the steady-state x_δ^s for a constant input $P_{\mathrm{d},\delta}^s$, i.e., $A x_\delta^s = P_{\mathrm{d},\delta}^s$. Standard algebraic manipulations reveal the steady-state model

$$\tilde{P}_{\mathrm{d},\delta}^s = -\mathrm{e}\tilde{b}_{12}^{\mathrm{ac}}\eta_{\delta,1}^s - (I_2 \otimes \mathbb{1}_2^{\mathsf{T}} L_{\mathrm{dc}} K_\omega^{-1} I_2 \otimes \mathbb{1}_2 + K_{\mathrm{g}})\omega_\delta^s, \quad (7)$$

where $\mathrm{e} := (1, -1)$, and $\tilde{P}_{\mathrm{d},\delta}^s := (P_{\mathrm{d},\delta,1}^s, P_{\mathrm{d},\delta,2}^s)$. In addition, if two ac areas are connected via an HVAC transmission line (i.e., $b_{12}^{\mathrm{ac}} \neq 0$) the steady state is synchronous, i.e.,

$$\tilde{\omega}_\delta^s := \omega_{\delta,1}^s = \omega_{\delta,2}^s \quad (8)$$

holds. The following proposition establishes the existence of a quasi-synchronous steady state if the losses g_{lk}^{dc} vanish.

Proposition 1. (Quasi-synchronous steady state) If $g_{lk}^{\mathrm{dc}} \to \infty$ for $(l, k) \in \{(1, 2), (3, 4)\}$ and two ac areas connected via

(1) one HVDC link, it holds that $\omega_{\delta,1}^s / \omega_{\delta,2}^s = k_{\omega,1} / k_{\omega,2}$ and $v_{\delta,1}^s = v_{\delta,2}^s$.
(2) two HVDC links, it holds that $\omega_{\delta,1}^s / \omega_{\delta,2}^s = (k_{\omega,2}^{-1} + k_{\omega,4}^{-1}) / (k_{\omega,1}^{-1} + k_{\omega,3}^{-1})$, $v_{\delta,l}^s / v_{\delta,l+1}^s = k_{\omega,l+1} / k_{\omega,l}$ for $l \in \{1, 2\}$.

Proof. When two ac areas are connected via one HVDC link, the steady state is obtained by removing states that correspond to the angle differences across the HVAC transmission line and the second HVDC link from (7). Then, (7) simplifies to $-(L_{\mathrm{dc}} K_\omega^{-1} + K_{\mathrm{g}})\omega_\delta^s = \tilde{P}_{\mathrm{d},\delta}^s$ and $\omega_{\delta,1}^s = -(P_{\mathrm{d},\delta,1}^s + P_{\mathrm{d},\delta,2}^s) / (k_{\mathrm{g},1} + k_{\mathrm{g},2})$ holds. Hence, we have

$$\omega_\delta^s = \frac{1}{\frac{k_{\mathrm{g},1} k_{\mathrm{g},2}}{\tilde{g}_{12}^{\mathrm{dc}}} + \frac{k_{\mathrm{g},1}}{k_{\omega,2}} + \frac{k_{\mathrm{g},2}}{k_{\omega,1}}} \begin{bmatrix} \frac{k_{\mathrm{g},2}}{\tilde{g}_{12}^{\mathrm{dc}}} + k_{\omega,2}^{-1} & k_{\omega,2}^{-1} \\ k_{\omega,1}^{-1} & \frac{k_{\mathrm{g},1}}{\tilde{g}_{12}^{\mathrm{dc}}} + k_{\omega,1}^{-1} \end{bmatrix} \tilde{P}_{\mathrm{d},\delta}^s.$$

By letting $g_{12}^{\mathrm{dc}} \to \infty$, it follows that $\tilde{g}_{12}^{\mathrm{dc}} \to \infty$ and we have

$$\omega_\delta^s = \frac{1}{k_{\mathrm{g},1} k_{\omega,2}^{-1} + k_{\mathrm{g},2} k_{\omega,1}^{-1}} \begin{bmatrix} k_{\omega,2}^{-1} \\ k_{\omega,1}^{-1} \end{bmatrix} (P_{\mathrm{d},\delta,1}^s + P_{\mathrm{d},\delta,2}^s).$$

Hence, $\omega_{\delta,1}^s / \omega_{\delta,2}^s = k_{\omega,1} / k_{\omega,2}$. Setting $\frac{\mathrm{d}}{\mathrm{d}t} v_{\delta,l} = 0$ for $l \in \{1, 2\}$, (5) becomes $\omega_{\delta,l}^s = k_{\omega,l} v_{\delta,l}^s$ and $v_{\delta,1}^s = v_{\delta,2}^s$ holds.

Next, if the two ac areas are only connected by two HVDC links (i.e., $b_{12}^{\mathrm{ac}} = 0$), (7) simplifies to $-(\tilde{G}_{\mathrm{dc}} + K_{\mathrm{g}})\omega_\delta^s = \tilde{P}_{\mathrm{d},\delta}$ with $\mathfrak{g}_1 = k_{\omega,1}^{-1}\tilde{g}_{12}^{\mathrm{dc}} + k_{\omega,3}^{-1}\tilde{g}_{34}^{\mathrm{dc}}$, $\mathfrak{g}_2 = k_{\omega,2}^{-1}\tilde{g}_{12}^{\mathrm{dc}} + k_{\omega,4}^{-1}\tilde{g}_{34}^{\mathrm{dc}}$, and

$$\tilde{G}_{dc} = \begin{bmatrix} \mathfrak{g}_1 & -\mathfrak{g}_2 \\ -\mathfrak{g}_1 & \mathfrak{g}_2 \end{bmatrix}. \quad (9)$$

Letting $g_{lk}^{\mathrm{dc}} \to \infty$ in $\omega_\delta^s = -(\tilde{G}_{\mathrm{dc}} + K_{\mathrm{g}})^{-1}\tilde{P}_{\mathrm{d},\delta}^s$ for $(l, k) \in \{(1, 2), (3, 4)\}$, item two follows from $\tilde{G}_{\mathrm{dc}} \to \infty$. □

A trivial consequence of Prop. 1 is that $\omega_{\delta,1}^s = \omega_{\delta,2}^s$ if $k_{\omega,1} = k_{\omega,2}$ (one HVDC link) and $\omega_{\delta,1}^s = \omega_{\delta,2}^s$ if $(k_{\omega,1}, k_{\omega,3}) = (k_{\omega,2}, k_{\omega,4})$ (two HVDC links), i.e., if the HVDC link losses can be neglected and the gains $k_{\omega,l}$ are identical, the two ac areas admit a quasi-synchronous steady-state.

4.2 Circulating power flow

Next, we investigate conditions that rule out circulating power flows. To this end, let $P_{\mathrm{in},\delta,l}$ and $P_{\mathrm{out},\delta,l}$ denote total steady-state power flow in and out of each area $l \in \{1, 2\}$.

Definition 1. (Circulating power) If the two ac areas $l \in \{1, 2\}$ are connected through more than one line we define the circulating power

$$P_{\mathrm{circ},\delta,l} := (|P_{\mathrm{in},\delta,l}| + |P_{\mathrm{out},\delta,l}| - |P_{\mathrm{in},\delta,l} - P_{\mathrm{out},\delta,l}|) / 2 \geq 0.$$

Notably, the circulating power flow is non-zero (i.e., $P_{\mathrm{circ},\delta,l} \neq 0$) if the first ac area is importing and exporting power from the second area through different lines. To avoid this undesirable effect, we develop conditions under which the steady-state circulating power flow is zero.

Proposition 2. (Zero circulating power) Consider the ac areas $l \in \{1, 2\}$ with governor gain $k_{\mathrm{g},l} \in \mathbb{R}_{\geq 0}$ and load disturbances $P_{\mathrm{d},\delta,l} \in \mathbb{R}_{\geq 0}$. The circulating power flow is zero if and only if the two ac areas are connected

(1) via HVAC and HVDC link and $k_{\omega,1} = k_{\omega,2}$, or
(2) via two HVDC links and $k_{\omega,1} / k_{\omega,2} = k_{\omega,3} / k_{\omega,4}$.

Proof. When two ac areas are connected via an HVAC line and HVDC link, then $P_{\mathrm{ac},5}^s = \tilde{b}_{12}^{\mathrm{ac}}\eta_{\delta,1}^s$. Next, let $\Delta := (k_{\omega,1}^{-1} - k_{\omega,2}^{-1})$ and $k_{\mathrm{g},\Sigma} := k_{\mathrm{g},1} + k_{\mathrm{g},2}$. Using (8) and solving (7) for $P_{\mathrm{ac},\delta,5}^s$ results in $P_{\mathrm{ac},\delta,5}^s = (k_{\mathrm{g},1} P_{\mathrm{d},\delta,2}^s - k_{\mathrm{g},2} P_{\mathrm{d},\delta,1}^s) / k_{\mathrm{g},\Sigma} + \tilde{g}_{12}^{\mathrm{dc}}\Delta\tilde{\omega}_\delta^s$. Moreover, $P_{\mathrm{in},\delta,1} = P_{\mathrm{ac},\delta,1}^s = -\tilde{g}_{12}^{\mathrm{dc}}\Delta\tilde{\omega}_\delta^s$ and we rewrite $P_{\mathrm{out},\delta,1} = P_{\mathrm{ac},\delta,5}^s = \mathcal{P} - P_{\mathrm{ac},\delta,1}^s$ where $\mathcal{P} := (k_{\mathrm{g},1} P_{\mathrm{d},\delta,2}^s - k_{\mathrm{g},2} P_{\mathrm{d},\delta,1}^s) / k_{\mathrm{d},\Sigma}$. Hence, $|P_{\mathrm{in},\delta,1} - P_{\mathrm{out},\delta,1}| = |-\mathcal{P}|$ and $0 \leq P_{\mathrm{circ},\delta,l} = (|P_{\mathrm{ac},\delta,1}^s| + |-\mathcal{P} - P_{\mathrm{ac},\delta,1}^s| - |\mathcal{P}|) / 2 \leq |P_{\mathrm{ac},\delta,l}^s| = |\tilde{g}_{12}^{\mathrm{dc}}\Delta\tilde{\omega}_\delta|$, and for any $\tilde{\omega}_\delta^s \in \mathbb{R}_{\geq 0}$, $P_{\mathrm{circ},\delta,1} = 0$ if and only if $\Delta = 0$, i.e., $k_{\omega,1} = k_{\omega,2}$. For two ac areas connected via two HVDC links we solve (7) for ω_δ^s obtaining $\omega_{\delta,1}^s = -(\mathfrak{g}_2(P_{\mathrm{d},\delta,1}^s + P_{\mathrm{d},\delta,2}^s) + k_{\mathrm{g},2} P_{\mathrm{d},\delta,1}^s) / D$, $\omega_{\delta,2}^s = -(\mathfrak{g}_1(P_{\mathrm{d},\delta,1}^s + P_{\mathrm{d},\delta,2}^s) + k_{\mathrm{g},1} P_{\mathrm{d},\delta,2}^s) / D$ with $\mathfrak{g}_1, \mathfrak{g}_2$ as in (9), and $D := (\mathfrak{g}_1 k_{\mathrm{g},2} + \mathfrak{g}_2 k_{\mathrm{g},1} + k_{\mathrm{g},1} k_{\mathrm{g},2})$. Next, $P_{\mathrm{in},\delta,1} = P_{\mathrm{ac},\delta,1}^s + P_{\mathrm{ac},\delta,3}^s$ and $P_{\mathrm{out},\delta,1} = 0$. Moreover, for $i \in \{1, 3\}$, $P_{\mathrm{ac},\delta,i}^s = -P_{\mathrm{ac},\delta,i+1}^s = -\tilde{g}_{ii+1}^{\mathrm{dc}}(\omega_{\delta,i} / k_{\omega,i} - \omega_{\delta,i+1} / k_{\omega,i+1})$ holds. Substituting ω_δ in $P_{\mathrm{ac},\delta,1}^s$, $P_{\mathrm{ac},\delta,3}^s$ and performing algebraic manipulations, we obtain $P_{\mathrm{ac},\delta,1}^s = \mathcal{P}_1 - \mathcal{P}_2$ and $P_{\mathrm{ac},\delta,3}^s = \mathcal{P}_3 + \mathcal{P}_2$ with $\mathcal{P}_2 = \tilde{g}_{12}^{\mathrm{dc}}\tilde{g}_{34}^{\mathrm{dc}}(P_{\mathrm{d},\delta,1}^s + P_{\mathrm{d},\delta,2}^s)(\gamma_{12} - \gamma_{34}) / (D k_{\omega,1} k_{\omega,3})$ and $\mathcal{P}_i = \tilde{g}_{ii+1}^{\mathrm{dc}}(k_{\mathrm{g},i+1} P_{\mathrm{d},\delta,1}^s - \gamma_{ii+1} k_{\mathrm{g},i} P_{\mathrm{d},\delta,2}) / (D k_{\omega,i})$ for $i \in \{1, 3\}$ and $\gamma_{lk} := k_{\omega,l} / k_{\omega,k}$, $(l, k) \in \{(1, 2), (3, 4)\}$. Consequently, $2 P_{\mathrm{circ},\delta,1} = |P_{\mathrm{ac},\delta,1}^s| + |P_{\mathrm{ac},\delta,3}^s| - |P_{\mathrm{ac},\delta,1}^s + P_{\mathrm{ac},\delta,3}^s| = |\mathcal{P}_1 - \mathcal{P}_2| + |\mathcal{P}_2 + \mathcal{P}_3| - |\mathcal{P}_1 + \mathcal{P}_3|$. Using the triangle inequality it follows that $P_{\mathrm{circ},\delta,1} = 0$ if and only $\gamma_{12} = \gamma_{34}$. □

5. FREQUENCY AND DC VOLTAGE STABILITY

Next, we investigate frequency and dc voltage stability.

5.1 Stability conditions

We require the following condition to ensure that at least one grid has a primary control response.

Condition 1. (Primary frequency response) At least one ac area has non-zero primary frequency control gain, i.e., there exists $l \in \{1, 2\}$ such that $k_{g,l} > 0$.

Moreover, we require the following sufficient condition.

Condition 2. (Control gains) Given $c_l \in \mathbb{R}_{>0}$, g_{lk}^{dc}, and $v_l^\star \in \mathbb{R}_{>0}$, for every pair of HVDC converters with index $(l, k) \in \{(1, 2), (3, 4)\}$ the control gains satisfy

$$\frac{g_{lk}^{dc}}{c_l} \frac{k_{p,l}}{k_{\omega,l}} < 2$$

For the system under consideration, $k_{\omega,l}$ parametrizes the steady-state mapping between dc voltage and ac frequency and is envisioned to be provided by the system operator. Moreover, the dc link losses g_{lk}^{dc} and VSC energy buffer c_l are typically fixed network and device parameters. Consequently, the derivative gain $k_{p,l}$ is the only remaining design parameter. In particular, smaller line losses, smaller energy buffer, or lower proportional gains $k_{\omega,l}$ all require smaller derivative gain.

5.2 Stability analysis

The next theorem provides conditions for asymptotic stability of (6) (i.e., with $P_{d,\delta} = \mathbb{0}_{13}$).

Theorem 3. (Asymptotic stability) Under Cond. 1 and Cond. 2, the system (6) is asymptotically stable if the two ac areas are connected

(1) via a single HVDC link,
(2) via HVAC and one HVDC link and $k_{\omega,1} = k_{\omega,2}$, or
(3) via two HVDC links and either $(k_{\omega,1}, k_{\omega,3}) = (k_{\omega,2}, k_{\omega,4})$ or $(k_{\omega,1}, k_{\omega,2}) = (k_{\omega,3}, k_{\omega,4})$ holds.

Proof. We will first consider the second case. The dynamics are obtained by excluding rows and columns corresponding to the second HVDC link (i.e., removing $v_{\delta,3}, v_{\delta,4}, \theta_{\delta,3}, \theta_{\delta,4}$). Next, assuming $k_{g,1}, k_{g,2} > 0$, we define the LaSalle function $V := x_\delta^\mathsf{T} \mathcal{V} x_\delta$ where $\mathcal{V} := \mathrm{diag}\{\mathcal{W}_{ac}, M, K_\omega C, T_g K_g^{-1}\}$. The time derivative of V is given by $\frac{d}{dt} V := -x_\delta^\mathsf{T} \mathcal{Q} x_\delta$ and

$$\mathcal{Q} := \begin{bmatrix} K_p C^{-1} \mathcal{W}_{ac}^2 & \mathbb{0}_{3\times 2} & \frac{-\mathcal{W}_{ac} K_p C^{-1} L_{dc}}{2} & \mathbb{0}_{3,2} \\ \mathbb{0}_{2\times 3} & \mathbb{0}_{2\times 2} & \mathbb{0}_{2\times 2} & \mathbb{0}_{2\times 2} \\ \frac{-L_{dc} K_p C^{-1} \mathcal{W}_{ac}}{2} & \mathbb{0}_{2\times 2} & \frac{K_\omega L_{dc} + L_{dc} K_\omega}{2} & \mathbb{0}_{2\times 2} \\ \mathbb{0}_{2\times 3} & \mathbb{0}_{2\times 2} & \mathbb{0}_{2\times 2} & K_g^{-1} \end{bmatrix},$$

Let $\tilde{L} := (K_{\omega,1} - L_{dc} K_p C^{-1}) L_{dc}$ and note that $\tilde{L} = \mathbb{e} \tilde{g}_{12}(k_{\omega,1} - \tilde{g}_{12}(k_{p,1}/(c_1 v_{12}^\star) + k_{p,2}/(c_2 v_{12}^\star))/4)\mathbb{e}^\mathsf{T}$ with $\mathbb{e} = (1, -1)$. If Cond. 2 holds, then $\tilde{L}$ is positive definite and, using Schur complement, it follows that $\frac{d}{dt} V \le 0$. The invariant set $\mathcal{E} := \{x_\delta \in \mathbb{R}^9 | \frac{d}{dt} V = 0\}$ can be rewritten as $\mathcal{E} = \{x_\delta \in \mathbb{R}^9 | \eta_\delta = \mathbb{0}_3, (v_{\delta,1}, v_{\delta,2}) = \alpha \mathbb{1}_2, \alpha \in \mathbb{R}, P_g = \mathbb{0}_2\}$. For the system dynamics on the maximal invariant set $\mathcal{S} \subseteq \mathcal{E}$, $\frac{d^k}{dt^k} \eta_\delta = \mathbb{0}_3$, $\frac{d^k}{dt^k} v_\delta = \mathbb{0}_2$ and $\frac{d^k}{dt^k} P_{g,\delta} = \mathbb{0}_2$ hold for all $k \in \mathbb{N}_0$. Moreover, it can be verified that the invariance conditions hold if and only if $x = \mathbb{0}_9$, i.e., $\mathcal{S} = \{\mathbb{0}_9\}$. Since $\mathcal{V}$ is positive definite and $\mathcal{Q}$ is positive semi-definite, it follows that all sublevel sets of V and system trajectories are bounded. Using LaSalle's invariance principle and linearity of the system, it follows that the maximal invariant set $\mathcal{S} = \{\mathbb{0}_9\}$ contained in $\frac{d}{dt} V = 0$ is (uniformly) asymptotically stable.
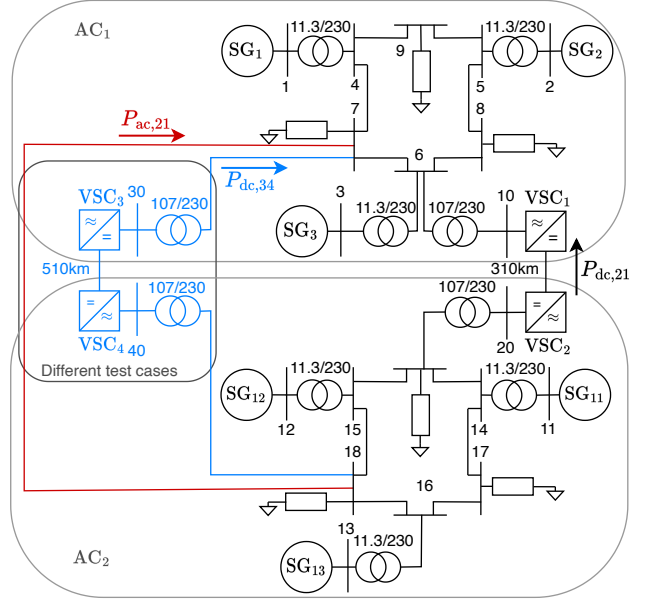

Fig. 2. Case study consisting of two IEEE9-bus systems (ac 1, ac 2), connected via i) the HVDC link at bus 10 (black), ii) the HVAC line at bus 7 (red), and iii) two HVDC links at bus 10 (black) and bus 7 (blue).

If either $k_{g,1} = 0$ or $k_{g,2} = 0$, then rows and columns of the corresponding variables are removed from $\mathcal{V}$ and $\mathcal{Q}$. Then, the states $P_{g,l}$ corresponding to l such that $k_{g,l} = 0$ are restricted to $\dot{P}_{g,l} = 0$. Using the same arguments as before, it can be shown that the equilibrium is (uniformly) asymptotically stable equilibrium of the system when $P_{g,l} = 0$ if $k_{g,l} = 0$. Moreover, the power generation, with zero governor gain (e.g., $T_{g,1} \frac{d}{dt} P_{g,\delta,1} = -P_{g,\delta,1}$) is trivially (uniformly) asymptotically stable. Then, the system is asymptotically stable because it is a cascaded interconnection of two asymptotically stable systems.

Next, we set $g_{34}^{dc} = 0$ and $b_{12}^{ac} = 0$, and redefine $\mathcal{V} := \mathrm{diag}\{\mathcal{W}_{ac} K_\omega^{-1}, M K_\omega^{-1}, C, K_{\omega,g}^{-1} K_g^{-1} T_g\}$. The first statement follows from the same argument as before.

Redefine $\mathcal{V} := \mathrm{diag}\{\mathcal{W}_{ac}, M, K_\omega C, T_g K_g^{-1}\}$ and Let $b_{12}^{ac} = 0$. Then, if $(k_{\omega,1}, k_{\omega,3}) = (k_{\omega,2}, k_{\omega,4})$ or $(k_{\omega,1}, k_{\omega,2}) = (k_{\omega,3}, k_{\omega,4})$, then $\mathcal{V} := \{\mathcal{W}_{ac} K_\omega, M K_1^{-1} C, K_1^{-1} K_g^{-1} T_g\}$, $K_1 := \mathrm{diag}\{k_{\omega,1}, k_{\omega,2}\}$. Then, using the same arguments as before, the third statement follows. $\square$

6. CASE STUDY

In this section, we use an EMT simulation of a high-fidelity case study to illustrate and verify the analytical results.

6.1 Benchmark system

We consider the test-case system, shown in Fig. 2, consisting of two IEEE-9 bus systems interconnected via an HVDC link connecting bus 10 and bus 20. An additional HVDC link and HVAC transmission line are modeled between bus 7 and bus 16. The synchronous generators (SGs) at bus 1, bus 2, bus 3, bus 11, bus 12, and bus 13 are modeled using an 8-th order synchronous machine model with standard exciter model, automatic voltage regulator, a multi band power system stabilizer, and a first-order turbine model with 5% speed droop. Each

HVDC converter is equipped with an RLC filter and cascaded inner current and voltage PI controls, with proportional and integral current gains $(k_p, k_i) = (3.1, 0.9)$, and voltage gains $(k_p, k_i) = (0.43, 0.69)$ in per unit. The SG and HVDC converters are connected to HVAC transmission through medium-voltage/high-voltage and high-voltage/high-voltage transformers, respectively. The HVAC lines and DC cables of length 310 km and 510 km are modeled using the standard π-line dynamics and transformers are explicitly modeled via dynamical models. Finally, the reference voltage phase angles of the HVDC converters are provided by (5) while the ac voltage magnitude reference is obtained using standard reactive power-voltage droop with 1% droop.

Finally, both areas have nominal frequency of $f_b = 50$ Hz, base power $S_b = 100$ MW, and the ac and dc voltage magnitudes are $V_b^{ac} = 230$ kV and $V_b^{dc} = 320$ kV. The remaining parameters can be found in (Subotić and Groß, 2022) and references therein.

6.2 A point-to-point HVDC link

First, we simulate the system shown in Fig. 2 with one HVDC link. For a constant $k_{p,l} = 0.001$ p.u., we vary $k_{\omega,1}/k_{\omega,2}$ to illustrate the impact on the steady-state power transfer. Moreover, for $k_{\omega,1} = k_{\omega,2} = 0.2$ p.u. we simulate load step and disconnecting an HVDC converter when the SG in ac 2 does not provide a frequency response.

Table 1. Active power-set points.

	SG_1	SG_2	SG_3	SG_{11}	SG_{12}	SG_{13}
$P^\star$ [p.u]	0.87	0.75	0.7	1	0.9	0.9

Steady-state response: The nominal active power set points are shown in Tab. 1, the nominal ac voltage magnitudes are 1 p.u., and the nominal dc voltage magnitudes are ≈ 1 p.u. with $v_2^\star - v_1^\star = 0.0035$ p.u., resulting in a nominal power flow of $P_{ac,1} \approx 0.23$ p.u. across the HVDC link. At $t = 5$s we simulate a load step of 0.2 p.u. at bus 8. Fig. 3 depicts the power across HVDC link for $k_{\omega,1}/k_{\omega,2} \in \{0.1, 0.5, 0.8, 1, 1.25, 10\}$. It can be seen that the sensitivity of one area to the disturbances in the other area scales with the ratio $k_{\omega,1}/k_{\omega,2}$. In particular, when $k_{\omega,1}/k_{\omega,2} = 10$, $\omega_{\delta,2} = 0.1\omega_{\delta,1}$ holds in the steady state and the change of the power flowing across the HVDC link is small. In contrast, $k_{\omega,1}/k_{\omega,2} = 0.1$ implies $\omega_{\delta,2} = 10\omega_{\delta,1}$ in steady state and results in a significant change in the power flow across the HVDC link.

Load perturbation and network resilience: The nominal operating point of the system is $P_1^\star = 0.84$ p.u., $P_2^\star = 0.8$ p.u., $P_3^\star = 0.7$ p.u and $P_{11}^\star = P_{12}^\star = P_{13}^\star = 1$ p.u with the ac voltage magnitudes of 1 p.u., and dc voltages ≈ 1 p.u. with $v_2^\star - v_1^\star = 0.003$ p.u.. At $t = 5$s a load step of 0.2 p.u. occurs at bus 17 and at $t = 30$ s VSC 2 is disconnected from ac 2. The results are shown in Fig. 4. It can be seen that, using identical proportional gains $k_{\omega,1} = k_{\omega,2}$, the two ac areas are quasi-synchronous, i.e., $\omega_1 \approx \omega_2$, up to the HVDC link losses. Finally, disconnecting VSC 2, the converter maintains stable frequency and dc voltage.

6.3 HVDC link and HVAC line connecting two ac areas

Next, we illustrate system behavior when the two ac areas are connected via an HVAC line and HVDC link
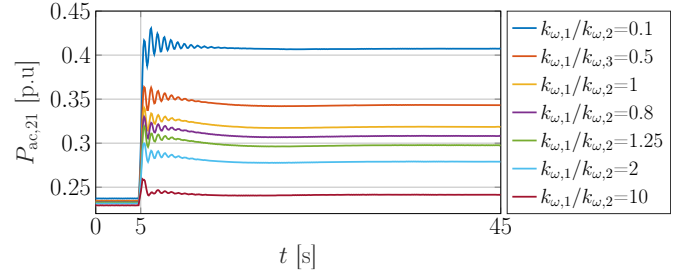

Fig. 3. Power flow across a single HVDC link connecting ac 1 and ac 2 for different ratios $k_{\omega,1}/k_{\omega,2}$.
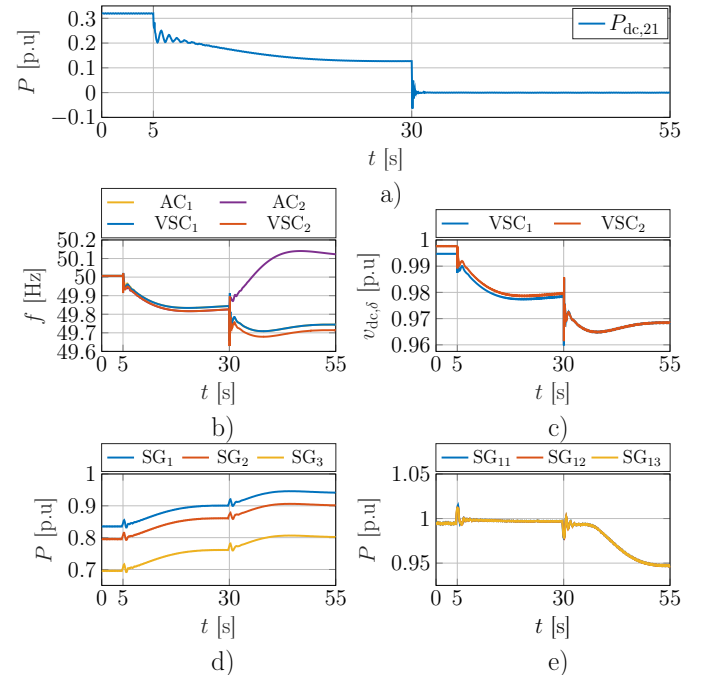

Fig. 4. Ac 1 and ac 2 connected through a single HVDC link with $k_{\omega,1} = k_{\omega,2}$: a) Power across the HVDC link, b) frequencies, c) dc voltages, d) power generation in ac 1, e) power generation in ac 2.

(cf. Fig. 2). The nominal operating point is given in Tab. 1 with ac voltage magnitudes of 1 p.u. and dc voltage magnitudes of ≈ 1 p.u and $v_2^\star - v_1^\star = 0.0039$ p.u. A 0.2 p.u. load step at bus 8 at $t = 5$ s is simulated. Simulation results for $k_{p,i} = 0.001$ p.u., $k_{\omega,1}/k_{\omega,2} = 1$ (left), and $k_{\omega,2}/k_{\omega,3} = 1$ (right) are shown in Fig. 5. The system behaves as expected and reduces the power export across the HVAC line from ac 1 to ac 2. The circulating power resulting from $k_{\omega,1}/k_{\omega,2} \in \{0.5, 1, 1.25, 2\}$ is shown in Fig. 6. As predicted by Prop. 2, the circulating power is only negligible if $k_{\omega,1}/k_{\omega,2} = 1$. Notably, as shown in Fig.5 e), even if the steady state exhibits a circulating power flow (e.g., due to misoperation of markets) the steady-state response to a load step does not result in any additional circulating power.

6.4 Two HVDC links connecting two areas

Finally, we illustrate system behavior when the two ac areas are only connected by two HVDC links (cf. Fig. 2). The nominal active power set points are shown in Tab. 1, the nominal ac voltage magnitudes are 1 p.u., and the dc voltage magnitudes are ≈ 1 p.u. with $v_k^\star - v_l^\star = 0.0039$ p.u.
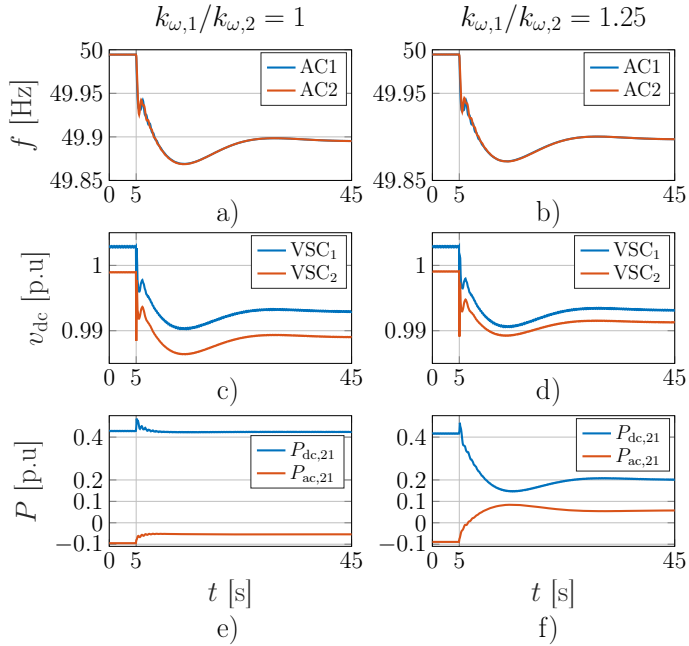
Fig. 5. Two ac areas connected via HVAC and HVDC: a), b) frequency, c), d) dc voltage, e) f) power across the HVAC line and HVDC link. The plots on the left correspond to $k_{\omega,1}/k_{\omega,2} = 1$, while the ones on the right correspond to $k_{\omega,1}/k_{\omega,2} = 1.25$.
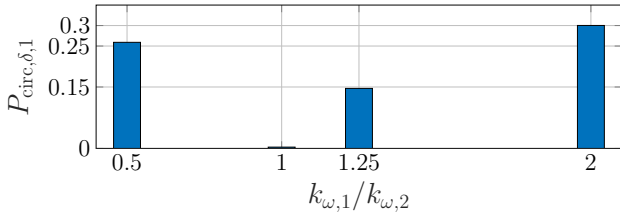

Fig. 6. Circulating power between two ac areas connected via an HVAC line and HVDC link.

for $(l,k) \in \{(1,2),(3,4)\}$. At $t = 5$s we simulate a load step of 0.2 p.u. at bus 8 for $(k_{\omega,l}, k_{\omega,l+2}) = (0.2, 0.25)$ p.u., $k_{p,l} = 0.001$ p.u. for $l \in \{1,2\}$. The simulation results are depicted in Fig. 7. As predicted by the theoretical analysis, the system is stable and a primary frequency response and inertia response are provided through the HVDC network. Moreover, the two ac areas connected through the two HVDC links are quasi-synchronous up to the negligible HVDC link losses (i.e., $\omega_1 \approx \omega_2$).

7. CONCLUSION

In this paper, we considered energy-balancing dual-port grid-forming control for HVDC systems. Notably, dual-port control does not require assigning grid-following and grid-forming controls to different converters, reduces system complexity, and makes the HVDC system more resilient. Moreover, under suitable conditions on the control gains, using dual-port GFM control renders asynchronous ac areas quasi-synchronous. Our main contribution are stability conditions for typical HVDC network topologies. Moreover, we performed a detailed steady-state analysis and developed conditions on the control gains that avoid circulating power through the HVDC network. A high-fidelity case study is used to illustrate and verify our
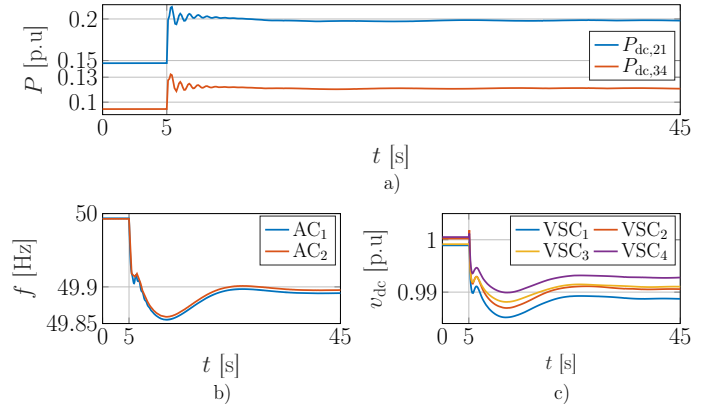

Fig. 7. Two ac areas connected via two HVDC links: a) HVDC power, b) frequency, and c) dc voltage.

theoretical analysis. Future work will consider more general network topologies, different types of generation, and consider a larger-scale case study.

REFERENCES

Chandorkar, M., Divan, D., and Adapa, R. (1993). Control of parallel connected inverters in standalone ac supply systems. *IEEE Trans. Ind. Appl.*, 29(1), 136–143.

D'Arco, S., Suul, J.A., and Fosso, O.B. (2015). A virtual synchronous machine implementation for distributed control of power converters in smartgrids. *Electr. Pow. Sys. Res.*, 122, 180–197.

Gomis-Bellmunt, O., Sánchez-Sánchez, E., Arévalo-Soler, J., and Prieto-Araujo, E. (2021). Principles of operation of grids of DC and AC subgrids interconnected by power converters. *IEEE Trans. Power Del.*, 36(2), 1107–1117.

Groß, D., Sanchez-Sanchez, E., Prieto-Araujo, E., and Gomis-Bellmunt, O. (2022). Dual-port grid-forming control of MMCs and its applications to grids of grids. *IEEE Trans. Power Del.*

Hertem, D.V., Gomis-Bellmunt, O., and Liang, J. (2016). *HVDC Grids HVDC for Offshore and Supergrid of the Future.* John Wiley & Sons, Ltd.

Lyu, X., Subotić, I., and Groß, D. (2022). Unified grid-forming control of PMSG wind turbines for fast frequency response and MPPT. In *Bulk Power System Dynamics and Control Symposium.*

Monshizadeh, P., De Persis, C., Stegink, T., Monshizadeh, N., and van der Schaft, A. (2017). Stability and frequency regulation of inverters with capacitive inertia. In *IEEE Conf. on Dec. and Contr.*, 5696–5701.

Mousavi, O.A., Bizumic, L., and Cherkaoui, R. (2013). Assessment of HVDC grid segmentation for reducing the risk of cascading outages and blackouts. In *Bulk Power System Dynamics and Control Symposium.*

Sauer, P.W. and Pai, M.A. (1998). *Power System Dynamics and Stability.* Prentice Hall.

Subotić, I. and Groß, D. (2022). Power-balancing dual-port grid-forming power converter control for renewable integration and hybrid ac/dc power systems. *IEEE Trans. Control Netw. Syst.*

Tayyebi, A., Groß, D., Anta, A., Kupzog, F., and Dörfler, F. (2020). Frequency stability of synchronous machines and grid-forming power converters. *IEEE Trans. Emerg. Sel. Topics Power Electron.*, 8(2), 1004–1018.